J Nanopart Res (2018) 20:184
https://doi.org/10.1007/s11051-018-4288-1

RESEARCH PAPER

Ruthenium nanoparticles cofunctionalized with acetylene derivatives of coumarin and perylene: dyad-like intraparticle charge transfer

Peiguang Hu · Yinghui Ren · Limei Chen · Fengqi Zhang · Yi Peng · Hsiau-Wei Lee · Shaowei Chen

Received: 22 February 2018 / Accepted: 29 June 2018

Abstract Nanoparticles are a unique structural scaffold for the fabrication of molecular dyad-like structures, in particular, when the functional moieties are bound onto the nanoparticle surface by conjugated interfacial bonds. In the present study, stable ruthenium nanoparticles (RuHC12) were prepared by the self-assembly of 1-dodecyne onto the nanoparticle surface forming ruthenium–vinylidene interfacial bonds and further functionalized with acetylene derivatives of coumarin and perylene by olefin metathesis reactions. Steady-state photoluminescence measurements of ethynylcoumarin-functionalized ruthenium (RuEC) nanoparticles showed that whereas the excitation and emission maxima remained almost unchanged, the normalized emission intensity was significantly enhanced, as compared to that of RuHC12, due to the much higher quantum yield of the coumarin moieties. By contrast, for the nanoparticles cofunctionalized with ethynylcoumarin and ethynylperylene (RuECEP), the excitation and emission maxima were close to those of ethynylperylene-functionalized ruthenium (RuEP) nanoparticles, but the normalized emissions of RuECEP were markedly quenched as compared to those of RuEP, due to effective photoinduced intraparticle charge transfer from the electron-donating coumarin moieties to the electro-accepting perylene moieties via the conjugated metal–ligand interfacial bonds in RuECEP. This is in sharp contrast to conventional coumarin–perylene dyads where energy transfer plays a dominant role and the perylene emissions were actually markedly enhanced. Consistent results were obtained in time-resolved fluorescence measurements, where RuECEP showed an emission lifetime (6.6 ns) that was longer than that of RuEP (5.0 ns), due to stabilization of the perylene excited state by the electron-donating coumarin groups.

Keywords Coumarin · Perylene · Photoluminescence · Interfacial bonding · Nanoparticle · Molecular dyad · Electron transfer

Peiguang Hu and Yinghui Ren contributed equally to this work.

Electronic supplementary material The online version of this article (https://doi.org/10.1007/s11051-018-4288-1) contains supplementary material, which is available to authorized users.

P. Hu · Y. Ren · L. Chen · Y. Peng · H.-W. Lee · S. Chen (✉)
Department of Chemistry and Biochemistry, University of California, 1156 High Street, Santa Cruz, CA 95064, USA
e-mail: shaowei@ucsc.edu

Y. Ren
School of Chemical Engineering, Northwest University, 229 North Taibai Road, Xi'an 710069 Shaanxi Province, China

F. Zhang
New Energy Research Institute, School of Environment and Energy, South China University of Technology, Guangzhou Higher Education Mega Center, Guangzhou 510007 Guangdong, China

Introduction

Molecular donor–acceptor dyads refer to a class of functional molecules consisting of an electron-donating moiety and an electron-accepting moiety bridged with a

Published online: 09 July 2018

covalent linker (Aviram and Ratner 1974). Upon photoirradiation, extensive intramolecular electron/energy transfer may occur and lead to the emergence of unprecedented optical and electronic properties, which can be exploited for diverse applications, such as solar energy conversion (Beaujuge et al. 2010; Bessho et al. 2010; Haid et al. 2012; Yao et al. 2015; Youngblood et al. 2009) and molecular electronics (Ashwell et al. 2010; Aviram and Ratner 1974, Jiang et al. 2004; Metzger 2003, Metzger et al. 1997; Raymo and Tomasulo 2005). For example, organic donor–acceptor dyads have been attracting extensive interest in the design and fabrication of efficient light-harvesting systems, primarily because of unidirectional charge transfer within the complexes, where the dynamics of intramolecular charge transfer has been found to be largely dictated by the structure of the chemical linker that bridges the electron-donating and electron-accepting groups (Agnihotri 2014, Espildora et al. 2014; Guan et al. 2015; Hanss et al. 2010). Molecular electronics, based on a donor–acceptor architecture, has been proposed for electrical current rectification since 1970s, due to asymmetric electrical responses to forward and reverse bias potentials (Aviram and Ratner 1974; Hedstrom et al. 2017) and dramatically reduced size of the electronic devices that may eventually replace silicon-based integrated circuits (Metzger 2003). Unfortunately, challenges remain in the application of this concept, including complex metal–ligand interfacial interactions, chemical and positional instabilities of the molecules, and so on (Kondratenko et al. 2011).

Recently, studies have shown that such dyad systems can be fabricated by using nanoparticles as part of the molecular architectures (Graff et al. 2016; Kotiaho et al. 2007, 2009; Lahav et al. 1999; Tel-Vered et al. 2008; Xu et al. 2010). One strategy is to exploit nanoparticles as a structural scaffold. For instance, Wilner et al. cross-linked gold nanoparticles with a Zn(II)–protoporphyrin IX–bipyridinium dyad forming a multilayer superstructure on an ITO electrode surface that exhibited three-dimensional conductivity and might be used as new electrode materials for photocells (Lahav et al. 1999). In another study (Kotiaho et al. 2007), Kotiaho et al. prepared a multilayer assembly of gold nanoparticles and porphyrin−fullerene dyads by the Langmuir–Schäfer technique and observed photoinduced vectorial electron transfer in the dyad, where the charge separation distance was found to increase by five folds when gold nanoparticles faced the porphyrin moiety of the dyad. This was accounted for by electron transfer from the porphyrin to the fullerene within the dyad followed by a secondary hole transfer from the porphyrin to the gold nanoparticles. In a further study (Kotiaho et al. 2009), Kotiaho and coworkers showed that both the photoluminescence emission and photoelectrical response of the porphyrin−fullerene dyads could be modified by long-range interactions with the gold nanoparticles. In these studies, the composite thin films were mostly prepared by noncovalent interactions between the nanoparticles and the molecular dyads.

Another strategy for the design and fabrication of dyad structures entails nanoparticles as electron donors and/or acceptors. One typical kind of such dyads consists of metal nanoparticles functionalized with fluorescent ligands, where the fluorophore photoemissions may be effectively quenched by the metal nanoparticles through energy/electron transfer (Xu et al. 2010). In some other studies, nanoparticle-based dyads are constructed by covalent linking of two nanoparticles, one as electron donor and the other as electron acceptor. For instance, Waldeck and coworkers fabricated a nanoscale dyad by covalently linking CdSe and CdTe quantum dots, where the quantum dot band edges were engineered for efficient interparticle electron transfer.

Dyad structures can also be prepared by concurrently, and yet independently, incorporating electron-donating and electron-accepting moieties onto the nanoparticle surface, where the metal–ligand interfacial bonds play a critical role in the determination of the dynamics of intraparticle charge transfer. For instance, in a recent study (Phebus et al. 2013), we cofunctionalized ruthenium nanoparticles with 4-ethynyl-*N*,*N*-diphenylaniline (EDPA, electron donor) and vinylanthracene (VAN, electron acceptor) through ruthenium–carbene π bonds, and observed effective charge transfer from the particle-bound EDPA to VAN moieties upon photoirradiation, a behavior analogous to that of conventional donor–acceptor molecular dyads. In photoluminescence study, the emissions of the cofunctionalized Ru(EDPA/VAN) nanoparticles suggested apparent mixing of the electronic energy levels of the EDPA and VAN moieties due to intraparticle charge delocalization facilitated by the conjugated metal–ligand interfacial bonds (Hu et al. 2016b). Photoelectrochemical studies showed that the voltammetric peaks of surface-bound EDPA diminished markedly under UV photoirradiation, due to the depletion of valence electrons of the photoexcited triphenylamine moieties, as a result of photoinduced electron transfer to the electron-accepting anthracene moieties (Lakowicz 2006; Nad and Pal 2000; Sauer et al. 1998; Singh et al. 2000; Vos and Engelborghs 1994).

Herein, we extend the study to the coumarin–perylene pair by cofunctionalization of ruthenium nanoparticles with 3-ethynylcoumarin (EC) and 9-ethynylperylene (EP). Note that coumarin–perylene molecular dyads have been prepared previously where the coumarin moiety serves as the electron donor and perylene as the electron acceptor. Because of a substantial spectral overlap of the coumarin emission and perylene absorption, efficient energy transfer has been observed leading to enhanced emission of the perylene moiety (Augulis et al. 2007; Hurenkamp et al. 2007; Serin et al. 2002). Interestingly, in the present study, when both the EC and EP ligands were bound onto ruthenium nanoparticle surface through conjugated ruthenium–vinylidene interfacial bonds, the EP emissions were actually found to be quenched markedly instead, along with a somewhat prolonged lifetime. This was accounted for by effective intraparticle charge delocalization that facilitated directional electron transfer from EC to EP.

Experimental section

Chemicals Ruthenium chloride ($RuCl_3$, ACROS), 1-dodecyne (HC12, 98%, Sigma Aldrich), 3-ethynylperylene (EP, > 95%, Abcam), 3-acetylcoumarin (98+%, Alfa Aesar), phosphorus oxychloride ($POCl_3$, 99%, Sigma Aldrich), *p*-dioxane (99%, T. J. Baker), and sodium acetate trihydrate ($NaOAc{\cdot}3H_2O$, MC&B) were all used as received. All solvents were obtained from typical commercial sources at their highest purity and used without further treatment. Water was supplied by a Barnstead Nanopure water system (18.3 MΩ cm).

Synthesis of 3-ethynylcoumarin EC was synthesized by adopting a literature procedure (El-Deen 1998, Mohamed et al. 2012). In brief, 3-acetylcoumarin (10 mmol) was dissolved in 10 mL of DMF purged with N_2 and cooled in an ice bath, into which a mixture of DMF and $POCl_3$ (2:1 M ratio) was added dropwise with the temperature controlled at 0 °C. The resulting mixture was stirred for 2 h in the ice bath and another 3 h at 65 °C before being poured onto crushed ice. The formed solids were filtered, washed with Nanopure water, and dried in vacuum. The dried solids were redissolved in 30 mL of *p*-dioxane and added into a boiling aqueous solution of sodium hydroxide (25 mL, 1 M). The mixed solution was refluxed for 45 min before being cooled down to room temperature and neutralized with hydrochloric acid (1 M). The mixture was then condensed by rotary evaporation, and the resulting solids were dispersed into CH_2Cl_2 and filtered. The filtrate was collected and dried with rotary evaporation, affording EC. FTIR measurements showed several characteristic peaks at 3241 cm^{-1} (≡C–H), 3071 cm^{-1} (aromatic =C–H), 3035 cm^{-1} (vinyl =C–H), 2107 cm^{-1} (C≡C), 1721 cm^{-1} (C=O), 1635 cm^{-1} (vinyl C=C), and 1607 cm^{-1} (aromatic C=C).

Synthesis of ruthenium nanoparticles Ruthenium nanoparticles capped with 1-dodecyne were prepared by following a procedure reported previously (Chen et al. 2006, 2008, 2009, 2010b). Briefly, 0.56 mmol (160 mg) of $RuCl_3$ and 4 mmol (328 mg) of NaOAc were added into 250 mL of 1,2-propanediol. The mixed solution was heated at 165 °C under vigorous stirring for 1 h. The solution color was found to change to dark brown, signifying the formation of "bare" ruthenium colloids. After the solution was cooled down to room temperature, 1.2 mmol of 1-dodecyne dissolved in 50 mL of toluene was added and the mixed solution was under magnetic stirring overnight. The toluene phase was then collected, dried with rotary evaporation, and rinsed extensively with a copious amount of acetonitrile to remove excess ligands, affording purified 1-dodecyne-capped ruthenium nanoparticles which were denoted as RuHC12. TEM measurements showed that the nanoparticles were rather monodisperse in size with an average diameter of ca. 2.2 nm (Fig. S1).

For further surface functionalization, the RuHC12 nanoparticles obtained above were dissolved in 4 mL of CH_2Cl_2 and divided into four equal aliquots. EC, EP, or a mixture (0.05 mmol) of EC and EP (1:1 M ratio) was added into three of the RuHC12 nanoparticle solutions for olefin metathesis reactions (Hu et al. 2016b) and stirred overnight. The solutions were then dried with N_2, rinsed with acetonitrile, and redissolved in CH_2Cl_2. The final products were denoted as ethynylcoumarin-functionalized ruthenium (RuEC), ethynylperylene-functionalized ruthenium (RuEP), and nanoparticles cofunctionalized with ethynylcoumarin and ethynylperylene (RuECEP) (Scheme 1), respectively.

Characterization Proton nuclear magnetic resonance (^1H NMR) measurements were conducted with a Varian Unity Inova 500 MHz NMR spectrometer. FTIR spectra were collected with a PerkinElmer Spectrum One FTIR spectrometer (spectral resolution 4 cm^{-1}), where the samples were prepared by drop casting the nanoparticle

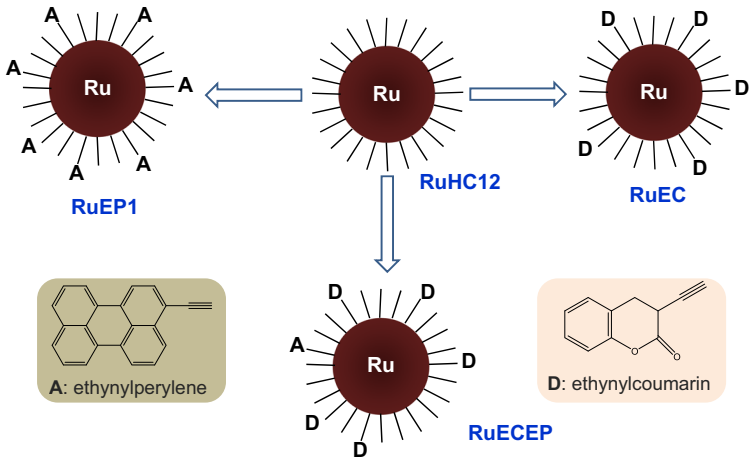

Scheme 1 Schematic of the preparation of RuEC, RuEP, and RuECEP nanoparticles based on olefin metathesis reactions

solutions onto a NaCl disk. UV–Vis spectra were collected with a PerkinElmer Lambda 35 UV–Vis spectrometer by using a quartz cuvette (1 cm × 1 cm) as the sample container at room temperature, and photoluminescence spectra were acquired with a FluoroMax-3 fluorospectrometer with the same solutions used for UV–Vis measurements. Time-resolved photoluminescence decay measurements were conducted using a Horiba QM3400 spectrometer with the pulsed laser excitation at 337 nm.

Results and discussion

Ruthenium nanoparticles functionalized with EC, EP, or both were prepared by olefin metathesis reactions of RuHC12 nanoparticles with the respective ligands (Scheme 1) (Hu et al. 2016b). The structures of the nanoparticle organic capping layers were first examined by ^{1}H NMR measurements. From Fig. 1, it can be seen that the RuHC12 nanoparticles (Scheme 1) exhibit two major, broad peaks at 0.89 and 1.27 ppm arising from the terminal methyl and methylene protons, respectively, of the 1-dodecyne ligands (the small peaks at 1.60, 5.31, and 7.26 ppm are from residual H_2O, CH_2Cl_2, and $CHCl_3$, respectively). After ligand exchange with EC, EP, and EC + EP mixture, new broad peaks emerged within the range of 5.5 to 9 ppm (figure inset), indicating successful functionalization of the ruthenium nanoparticles with the aromatic fluorophores. For the RuEC nanoparticles, the broad peak is centered at 7.31 ppm, due to the combined contributions of the EC phenyl and vinyl protons (Scheme 1) (El-Deen 1998; Mohamed et al. 2012). For the RuEP nanoparticles, two broadbands can be seen at 7.62, and 8.31 ppm, consistent with the aromatic protons in EP (Scheme 1). Similarly, RuECEP nanoparticles exhibited three broad peaks at 7.47, 7.62, and 8.27 ppm, due to the cofunctionalization of the nanoparticles by both EC and EP ligands (Scheme 1). In addition, based on the integrated peak areas, it was found that about 15.8% of the HC12 ligands were replaced by EC forming the RuEC nanoparticles; in RuEP nanoparticles, the surface coverage of EP was 22.8%, whereas in RuECEP nanoparticles, the surface coverages of EC and EP were estimated to be 17.1 and 6.1%, respectively, corresponding to an EC:EP molar ratio of 2.8:1. Furthermore, the fact that

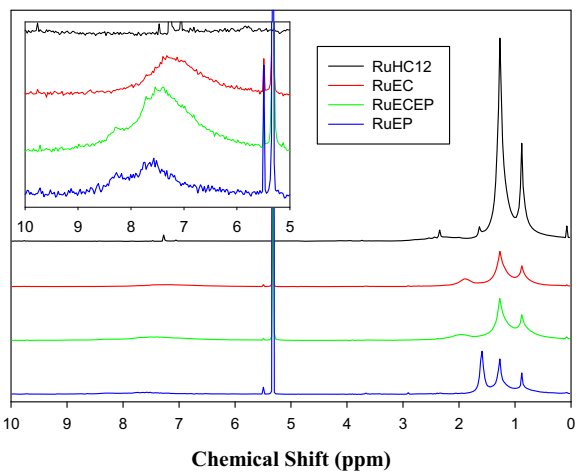

Fig. 1 ^{1}H NMR spectra of RuHC12 (black), RuEC (red), RuECEP (green), and RuEP (blue) nanoparticles in CD_2Cl_2. Figure inset magnifies the region between 5 and 10 ppm (color figure online)

no sharp spectral features were observed in any of the four nanoparticles indicates that the samples were spectroscopically clean and free of excess ligand monomers (Chen et al. 2006, 2008, 2009, 2010b). The incorporation of these aromatic ligands onto the nanoparticle surface was also evidenced in FTIR measurements (Fig. S2).

The optical properties of the series of nanoparticles were then characterized by UV–Vis and photoluminescence (PL) measurements. From the UV–Vis absorption spectra in Fig. 2a, one can see that the RuHC12 nanoparticles (black curve) exhibited a simple exponential decay profile, characteristic of transition–metal nanoparticles as described by the Mie theory (Creighton and Eadon 1991). In comparison, after exchange reactions with EC ligands, the resulting RuEC nanoparticles (red curve) exhibited two broadbands centered at 285 and 330 nm, due to the π–π* transitions of the EC ligands (Fig. S3A) (Abueittah and Eltawil 1985; Donovalova et al. 2012). For the RuEP nanoparticles (blue curve), three broadbands appear at 255, 425, and 450 nm, which arise from the π-π* transitions of the EP ligands (Fig. S3A) (Feng et al. 2005; Jain and Zaidi 1988; Lukas et al. 2002). These absorption features can all be clearly identified with the RuECEP nanoparticles (green curve), as both EC and EP ligands were incorporated onto the nanoparticle surface.

Figure 2b depicts the corresponding PL spectra, where the excitation spectra were acquired at the emission maximum and emission spectra at the corresponding excitation maximum, with the PL intensity normalized to the respective optical density at the excitation wavelength for each sample (Fig. 2a). One can see that the RuHC12 nanoparticle (Scheme 1) exhibited an excitation maximum (λ_{ex}) at 368 nm and an emission maximum (λ_{em}) at 447 nm, due to intraparticle charge delocalization among the particle-bound acetylene moieties such that the nanoparticles behaved analogously to diacetylene derivatives (−C≡C−C≡C−), as observed previously (Chen et al. 2010a; Hu et al. 2014, 2015, 2016a; Kang et al. 2010). After olefin metathesis reactions with EC ligands to replace part of the HC12 ligands, the excitation and emission peak positions for the resulting RuEC nanoparticles (Scheme 1) remained almost unchanged at $\lambda_{ex} = 375$ nm and $\lambda_{em} = 450$ nm, but the emission intensity was enhanced by 40%, as compared to that of the RuHC12 nanoparticles, due to the incorporation of more emissive coumarin moieties onto the nanoparticle surface. In addition, one may notice that the λ_{ex} and λ_{em} values of the RuEC nanoparticles were substantially red shifted as compared to those of the EC monomers ($\lambda_{ex} = 340$ nm and $\lambda_{em} = 400$ nm; Fig. S3B), which may be accounted for by intraparticle charge delocalization between the coumarin moieties due to conjugated metal–ligand bonds (Scheme 1). For the RuEP nanoparticles, the excitation and emission maxima can be identified at 460 and 515 nm, also exhibiting a small red shift as compared to those of the EP monomers (455 and 490 nm; Fig. S3B) (Chen et al. 2009). Interestingly, for the RuECEP nanoparticles, the excitation and emission maxima (green curves) appeared at 460 and 520 nm, respectively, close to those of RuEP nanoparticles, suggesting that the photoluminescence emission of the RuECEP nanoparticles at $\lambda_{ex} = 460$ nm was dominated by the perylene moieties (Table 1). In fact, the ratio of the emission intensities of RuEP versus RuECEP, $R_{em} = I_{em,\ RuEP}/I_{em,\ RuECEP}$, at $\lambda_{ex} = 460$ nm, is estimated to be 3.5:1, very close to the ratio (3.7:1) of the concentrations of EP moieties on the RuEP and RuECEP nanoparticle surfaces based on ^{1}H NMR measurements (Fig. 1). It should be noted that at this wavelength (460 nm), the absorption of the coumarin moieties is minimal and thus only the EP ligands were excited and contributed to the emission.

Interestingly, at shorter excitation wavelengths such as 343, 360, and 375 nm (Fig. 3; Table 2), which are close to the excitation maxima of RuHC12 and RuEC nanoparticles, the emission peak positions (λ_{em}) of RuEP and RuECEP nanoparticles remained almost invariant, again, indicative of the dominant contributions of the perylene moieties to the nanoparticle photoluminescence, whereas the R_{em} value increased markedly, signifying diminishing emission of the RuECEP nanoparticles. For instance, R_{em} was estimated to be 4.7:1 at $\lambda_{ex} = 343$ nm, corresponding to a quenching efficiency of 27%, as compared to that at $\lambda_{ex} = 460$ nm, and the quenching efficiencies were somewhat lower at 17 and 20% when the samples were excited at $\lambda_{ex} = 360$ and 375 nm, respectively (Table 2). This might be accounted for by effective photoinduced intraparticle charge transfer from the particle-bound coumarin (electron donor at excited state) to perylene (electron acceptor) moieties through conjugated metal–vinylidene bonds and conductive metal cores, leading to apparent quenching of the photoluminescence emission of particle-bound perylene moieties (Jones et al. 1984; Lakowicz 2006; Nad and Pal 2000; Sauer

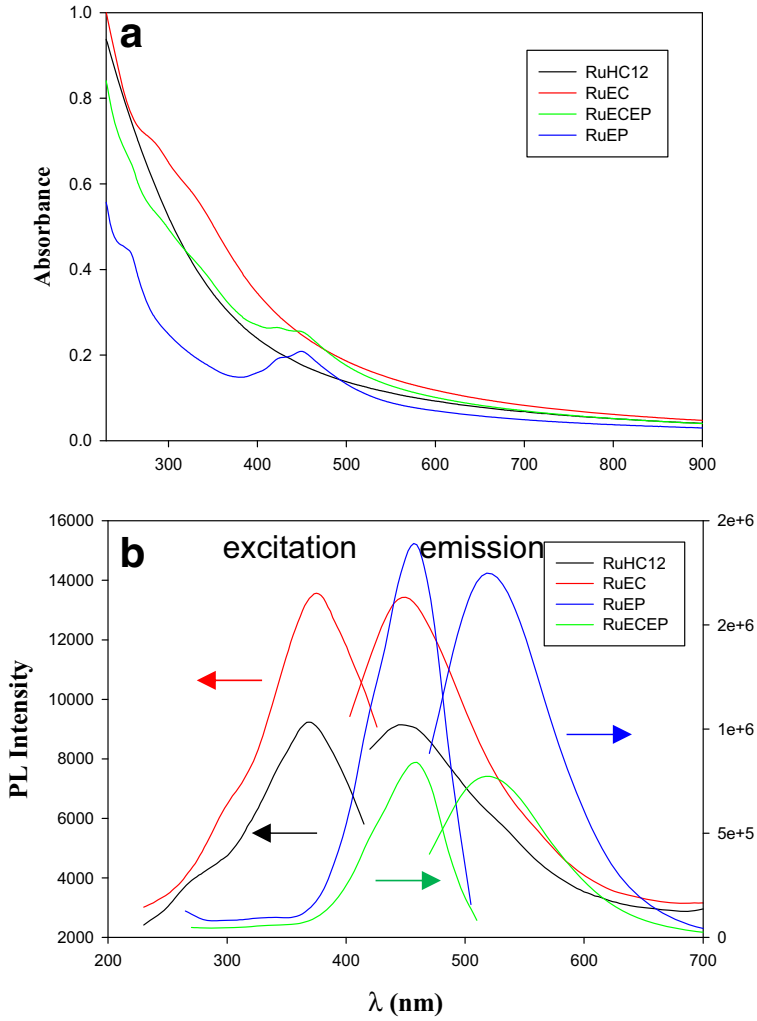

Fig. 2 **a** UV–Vis absorption and **b** photoluminescence spectra of RuHC12 (black), RuEC (red), RuEP (blue), and RuECEP (green) nanoparticles in CH_2Cl_2. In **b**, the intensity is normalized to the respective optical density at the excitation wavelength from the UV–Vis measurements in **a** (color figure online)

et al. 1998; Singh et al. 2000; Vos and Engelborghs 1994). In fact, the most efficient quenching was observed at $\lambda_{ex} = 343$ nm, which is close to the maximum absorption of the EC ligands (340 nm; Fig. S3A) leading to the most apparent charge transfer to the particle-bound EP moieties and quenching of the PL emissions (Chen et al. 2010a; Hu et al. 2014, 2015; Kang et al. 2010). This is consistent with results in the previous study with Ru(EDPA/VAN) nanoparticles where the particle-bound EDPA and VAN behaved analogously to the conventional molecular dyads (Phebus et al. 2013). In comparison, no quenching was observed with a simple mixture of EC and EP monomeric ligands in solution; to the contrary, the emission at 492 nm of the EC and EP mixed solution was actually enhanced (Table S1), as compared to that of the EP monomer solution at the same concentration, in good agreement with results in previous studies with coumarin–perylene dyads, where the enhanced emission of perylene was ascribed to effective energy transfer from the coumarin moiety (Augulis et al. 2007; Hurenkamp et al. 2007; Serin et al. 2002).

Taken together, these results suggest that effective intraparticle charge transfer occurred from the photoexcited, particle-bound coumarin to perylene moieties in RuECEP nanoparticles as a result of conjugated metal–

Table 1 Summary of the excitation (λ_{ex}) and emission (λ_{em}) peak positions of the various samples

Sample	EC	EP	RuHC12	RuEC	RuEP	RuECEP
λ_{ex} (nm)	340	455	368	375	460	460
λ_{em} (nm)	400	490	447	450	515	520

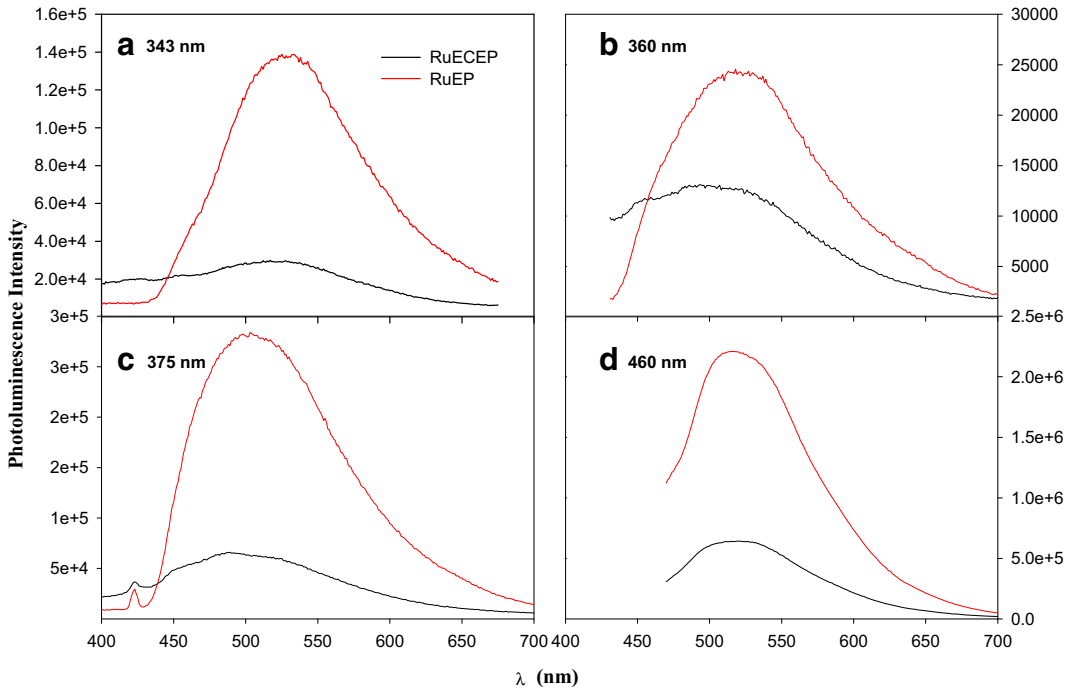

Fig. 3 Normalized emission profiles of RuEP (red) and RuECEP (black) nanoparticles excited at different wavelengths. **a** 343 nm. **b** 360 nm. **c** 375 nm. **d** 460 nm

ligand interfacial bonding interactions, whereas in conventional coumarin–perylene dyads, through-space energy transfer, rather than electron transfer, is the leading mechanism (Lakowicz 2006; Nad and Pal 2000; Sauer et al. 1998; Singh et al. 2000; Vos and Engelborghs 1994).

Consistent results were obtained with time-resolved PL measurements. Figure 4 shows the PL decay spectra measured at $\lambda_{ex} = 337$ nm for the EP monomers, RuEP, and RuECEP nanoparticles (the PL emission of RuEC nanoparticle was too weak for time-resolved analysis), where the decay profiles may be best fitted by a single exponential function, $f = a + be^{-t/\tau}$. From the fitting, the fluorescence lifetimes (τ) for the EP monomers, RuEP, and RuECEP nanoparticles are estimated to be 4.9 ± 0.1, 5.0 ± 0.1, and 6.6 ± 0.2 ns, respectively, in good agreement with results reported in the literature for perylene derivatives (Aigner et al. 2014; Ware and Cunningham 1966). The fact that the emission lifetime of RuECEP was actually longer than that of RuEP may be ascribed to the stabilization of the perylene groups by the photo-excited coumarin moieties, a behavior analogous to those reported previously where electron-donating

Table 2 Excitation and emission maxima, normalized emission intensities, and ratios of the emission intensities of RuEP and RuECEP nanoparticles, as well as calculated quenching efficiency

$\lambda_{ex}/\lambda_{em}$ (nm)	R_{em}	Quenching efficiency (%)
343/520	4.7:1	27
360/515	4.1:1	17
375/505	4.3:1	20
460/515	3.5:1	

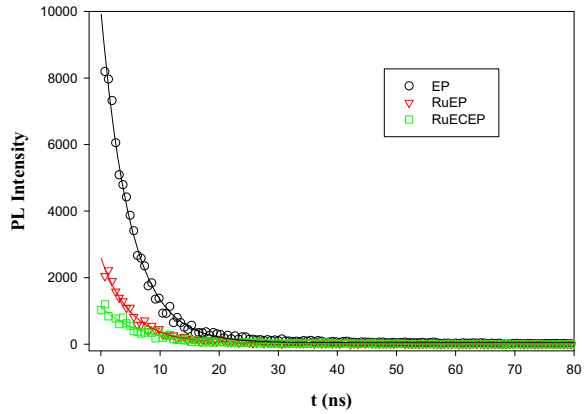

Fig. 4 Photoluminescence emission decay profiles of EP monomers, RuEP, and RuECEP nanoparticles at $\lambda_{ex} = 337$ nm. Symbols are experimental data and solid curves are single exponential fits where the R^2 coefficient is 0.996 for EP, 0.987 for RuEP, and 0.969 for RuECEP

substituents increased the excited state lifetime of perylene derivatives (Hight et al. 2013; Patra et al. 2012). This further supports the hypothesis that photo-induced electron transfer occurred from particle-bound coumarin to perylene moieties that was facilitated by the conjugated metal–ligand interfacial bonds (Lakowicz 2006; Nad and Pal 2000; Sauer et al. 1998; Singh et al. 2000; Vos and Engelborghs 1994).

In addition, the somewhat longer lifetimes of both RuEP and RuECEP than that of EP monomers can be attributed to the more rigid chemical environment surrounding the perylene moieties (Scheme 1), which is created by the neighboring organic protecting ligands and thus prolongs the lifetime of the excited state, as observed previously (Chen et al. 2009).

Conclusions

In this study, ruthenium nanoparticles were cofunctionalized with (electron-donating) coumarin and (electron-accepting) perylene moieties by olefin metathesis reactions of alkyne-capped nanoparticles with EC and EP ligands. Steady-state photoluminescence measurements showed that the excitation and emission maxima of the cofunctionalized RuECEP nanoparticles were actually close to those of the monofunctionalized RuEP counterparts, but with markedly quenched emissions, due to effective photoinduced intraparticle charge transfer from the coumarin groups to the perylene moieties through conjugated metal–vinylidene bonds and conductive ruthenium nanoparticle cores. Such a behavior is unlike that of a conventional coumarin–perylene molecular dyad, where the fluorescence of the perylene moiety actually increases due to energy transfer from the coumarin groups. This was further confirmed by time-resolved photoluminescence experiments, where RuECEP exhibited a somewhat longer lifetime than RuEP, as intraparticle charge transfer from the particle-bound coumarin helped stabilize the perylene excited state, akin to perylene derivatives with electron-donating substituents. These results further highlight the effectiveness of conjugated metal–ligand interfacial bonding interactions in facilitating intraparticle charge transfer, a unique characteristic that may be exploited for the fabrication of stable nanoparticle-mediated donor–acceptor dyads for diverse applications such as solar energy conversion and molecular electronics.

Acknowledgments TEM work was carried out at the National Center for Electron Microscopy, Lawrence Berkeley National Laboratory, which is supported by the US Department of Energy, as part of a user project.

Funding This work was supported, in part, by the National Science Foundation (CHE-1710408).

Compliance with ethical standards

Conflict of interest The authors declare that they have no conflict of interest.

References

Abueittah RH, Eltawil BAH (1985) The electronic absorption-spectra of some Coumarins—a molecular-orbital treatment. Can J Chem 63:1173–1179

Agnihotri N (2014) Computational studies of charge transfer in organic solar photovoltaic cells: a review. J Photochem Photobiol C Photochem Rev 18:18–31

Aigner D, Dmitriev RI, Borisov SM, Papkovsky DB, Klimant I (2014) pH-sensitive perylene bisimide probes for live cell fluorescence lifetime imaging. J Mater Chem B 2:6792–6801

Ashwell GJ, Urasinska-Wojcik B, Phillips LJ (2010) In situ stepwise synthesis of functional multijunction molecular wires on gold electrodes and gold nanoparticles. Angew Chem Int Ed 49:3508–3512

Augulis R, Pugzlys A, Hurenkamp JH, Feringa BL, van Esch JH, van Loosdrecht PHM (2007) Optical energy transport and interactions between the excitations in a coumarin-perylene bisimide dendrimer. J Phys Chem A 111:12944–12953

Aviram A, Ratner MA (1974) Molecular rectifiers. Chem Phys Lett 29:277–283

Beaujuge PM, Amb CM, Reynolds JR (2010) Spectral engineering in pi-conjugated polymers with intramolecular donor-acceptor interactions. Acc Chem Res 43:1396–1407

Bessho T, Zakeeruddin SM, Yeh CY, Diau EWG, Gratzel M (2010) Highly efficient mesoscopic dye-sensitized solar cells based on donor-acceptor-substituted porphyrins. Angew Chem Int Ed 49:6646–6649

Chen W, Davies JR, Ghosh D, Tong MC, Konopelski JP, Chen SW (2006) Carbene-functionalized ruthenium nanoparticles. Chem Mater 18:5253–5259

Chen W, Chen SW, Ding FZ, Wang HB, Brown LE, Konopelski JP (2008) Nanoparticle-mediated intervalence transfer. J Am Chem Soc 130:12156–12162

Chen W, Zuckerman NB, Lewis JW, Konopelski JP, Chen SW (2009) Pyrene-functionalized ruthenium nanoparticles: novel fluorescence characteristics from Intraparticle extended conjugation. J Phys Chem C 113:16988–16995

Chen W, Zuckerman NB, Kang XW, Ghosh D, Konopelski JP, Chen SW (2010a) Alkyne-protected ruthenium nanoparticles. J Phys Chem C 114:18146–18152

Chen W, Zuckerman NB, Konopelski JP, Chen SW (2010b) Pyrene-functionalized ruthenium nanoparticles as effective

chemosensors for nitroaromatic derivatives. Anal Chem 82: 461–465

Creighton JA, Eadon DG (1991) Ultraviolet visible absorption-spectra of the colloidal metallic elements. J Chem Soc Faraday Trans 87:3881–3891

Donovalova J, Cigan M, Stankovicova H, Gaspar J, Danko M, Gaplovsky A, Hrdlovic P (2012) Spectral properties of substituted Coumarins in solution and polymer matrices. Molecules 17:3259–3276

El-Deen IM (1998) A novel synthesis of coumarin derivatives. Chin J Chem 16:528–532

Espildora E, Delgado JL, Martin N (2014) Donor-acceptor hybrids for organic electronics. Isr J Chem 54:429–439

Feng W, Fujii A, Ozaki M, Yoshino K (2005) Perylene derivative sensitized multi-walled carbon nanotube thin film. Carbon 43:2501–2507

Graff BM, Bloom BP, Wierzbinski E, Waldeck DH (2016) Electron transfer in nanoparticle dyads assembled on a colloidal template. J Am Chem Soc 138:13260–13270

Guan L, Zhang XY, Sun FQ, Jiang Y, Zhong YP, Liu P (2015) Oligothiophene derivatives in organic photovoltaic devices. Prog Chem 27:1435–1447

Haid S, Marszalek M, Mishra A, Wielopolski M, Teuscher J, Moser JE, Humphry-Baker R, Zakeeruddin SM, Gratzel M, Bauerle P (2012) Significant improvement of dye-sensitized solar cell performance by small structural modification in pi-conjugated donor-acceptor dyes. Adv Funct Mater 22:1291–1302

Hanss D, Walther ME, Wenger OS (2010) Importance of covalence, conformational effects and tunneling-barrier heights for long-range electron transfer: insights from dyads with oligo-p-phenylene, oligo-p-xylene and oligo-p-dimethoxybenzene bridges. Coord Chem Rev 254:2584–2592

Hedstrom S, Matula AJ, Batista VS (2017) Charge transport and rectification in donor-acceptor dyads. J Phys Chem C 121: 19053–19062

Hight LM, McGuire MC, Zhang Y, Bork MA, Fanwick PE, Wasserman A, McMillin DR (2013) π donation and its effects on the excited-state lifetimes of luminescent platinum(II) terpyridine complexes in solution. Inorg Chem 52:8476–8482

Hu PG, Song Y, Rojas-Andrade MD, Chen SW (2014) Platinum nanoparticles functionalized with ethynylphenylboronic acid derivatives: selective manipulation of nanoparticle photoluminescence by fluoride ions. Langmuir 30:5224–5229

Hu PG, Duchesne PN, Song Y, Zhang P, Chen SW (2015) Self-assembly and chemical reactivity of alkenes on platinum nanoparticles. Langmuir 31:522–528

Hu PG, Chen LM, Deming CP, Kang XW, Chen SW (2016a) Nanoparticle-mediated Intervalence charge transfer: core-size effects. Angew Chem Int Ed 55:1455–1459

Hu PG, Chen LM, Kang XW, Chen SW (2016b) Surface functionalization of metal nanoparticles by conjugated metal-ligand interfacial bonds: impacts on Intraparticle charge transfer. Acc Chem Res 49:2251–2260

Hurenkamp JH, Browne WR, Augulis R, Pugzlys A, van Loosdrecht PHM, van Esch JH, Feringa BL (2007) Intramolecular energy transfer in a tetra-coumarin perylene system: influence of solvent and bridging unit on electronic properties. Org Biomol Chem 5:3354–3362

Jain VK, Zaidi ZH (1988) A re-investigation of the electronic-spectrum of perylene. Spectrochim Acta A 44:1159–1163

Jiang P, Morales GM, You W, Yu LP (2004) Synthesis of diode molecules and their sequential assembly to control electron transport. Angew Chem Int Ed 43:4471–4475

Jones G, Griffin SF, Choi CY, Bergmark WR (1984) Electron donor-acceptor quenching and photoinduced electron-transfer for Coumarin dyes. J Org Chem 49:2705–2708

Kang XW, Zuckerman NB, Konopelski JP, Chen SW (2010) Alkyne-stabilized ruthenium nanoparticles: manipulation of Intraparticle charge delocalization by nanoparticle charge states. Angew Chem Int Ed 49:9496–9499

Kondratenko M, Moiseev AG, Perepichka DF (2011) New stable donor-acceptor dyads for molecular electronics. J Mater Chem 21:1470–1478

Kotiaho A, Lahtinen RM, Tkachenko NV, Efimov A, Kira A, Imahori H, Lemmetyinen H (2007) Gold nanoparticle enhanced charge transfer in thin film assemblies of porphyrin-fullerene dyads. Langmuir 23:13117–13125

Kotiaho A, Lahtinen R, Latvala HK, Efimov A, Tkachenko NV, Lemmetyinen H (2009) Effect of gold nanoparticles on intramolecular exciplex emission in organized porphyrin-fullerene dyad films. Chem Phys Lett 471:269–275

Lahav M, Gabriel T, Shipway AN, Willner I (1999) Assembly of a Zn(II)-porphyrin-bipyridinium dyad and Au-nanoparticle superstructures on conductive surfaces. J Am Chem Soc 121: 258–259

Lakowicz JR (2006) Principles of fluorescence spectroscopy. Springer, New York

Lukas AS, Zhao YY, Miller SE, Wasielewski MR (2002) Biomimetic electron transfer using low energy excited states: a green perylene-based analogue of chlorophyll a. J Phys Chem B 106:1299–1306

Metzger RM (2003) Unimolecular electrical rectifiers. Chem Rev 103:3803–3834

Metzger RM, Chen B, Hopfner U, Lakshmikantham MV, Vuillaume D, Kawai T, Wu XL, Tachibana H, Hughes TV, Sakurai H, Baldwin JW, Hosch C, Cava MP, Brehmer L, Ashwell GJ (1997) Unimolecular electrical rectification in hexadecylquinolinium tricyanoquinodimethanide. J Am Chem Soc 119:10455–10466

Mohamed HM, Abd El-Wahab AHF, Ahmed KA, El-Agrody AM, Bedair AH, Eid FA, Khafagy MM (2012) Synthesis, reactions and antimicrobial activities of 8-ethoxycoumarin derivatives. Molecules 17:971–988

Nad S, Pal H (2000) Electron transfer from aromatic amines to excited coumarin dyes: fluorescence quenching and picosecond transient absorption studies. J Phys Chem A 104:673–680

Patra D, Malaeb NN, Haddadin MJ, Kurth MJ (2012) Influence of substituent and solvent on the radiative process of singlet excited states of novel cyclic azacyanine derivatives. J Fluoresc 22:707–717

Phebus BD, Yuan Y, Song Y, Hu PG, Abdollahian Y, Tong QX, Chen SW (2013) Intraparticle donor-acceptor dyads prepared using conjugated metal-ligand linkages. Phys Chem Chem Phys 15:17647–17653

Raymo FM, Tomasulo M (2005) Electron and energy transfer modulation with photochromic switches. Chem Soc Rev 34:327–336

Sauer M, Drexhage KH, Lieberwirth U, Muller R, Nord S, Zander C (1998) Dynamics of the electron transfer reaction between an oxazine dye and DNA oligonucleotides monitored on the single-molecule level. Chem Phys Lett 284:153–163

Serin JM, Brousmiche DW, Frechet JMJ (2002) A FRET-based ultraviolet to near-infrared frequency converter. J Am Chem Soc 124:11848–11849

Singh MK, Pal H, Sapre AV (2000) Interaction of the excited singlet state of neutral red with aromatic amines. Photochem Photobiol 71:300–306

Tel-Vered R, Yehezkeli O, Yildiz HB, Wilner OI, Willner I (2008) Photoelectrochemistry with ordered CdS nanoparticle/relay or photosensitizer/relay dyads on DNA scaffolds. Angew Chem Int Ed 47:8272–8276

Vos R, Engelborghs Y (1994) A fluorescence study of tryptophan histidine interactions in the peptide anantin and in solution. Photochem Photobiol 60:24–32

Ware WR, Cunningham PT (1966) Fluorescence lifetime and fluorescence enhancement of perylene vapor. J Chem Phys 44:4364–4365

Xu JP, Jia L, Fang YA, Lv LP, Song ZG, Ji JA (2010) Highly soluble PEGylated pyrene-gold nanoparticles dyads for sensitive turn-on fluorescent detection of biothiols. Analyst 135:2323–2327

Yao ZY, Zhang M, Wu H, Yang L, Li RZ, Wang P (2015) Donor/acceptor indenoperylene dye for highly efficient organic dye-sensitized solar cells. J Am Chem Soc 137:3799–3802

Youngblood WJ, Lee SHA, Maeda K, Mallouk TE (2009) Visible light water splitting using dye-sensitized oxide semiconductors. Acc Chem Res 42:1966–1973